Comparative Analysis of Transverse Mode Instability in Single-Clad and Double-Clad Fibers

Elbis Santos Cardoso
University of São Paulo
São Paulo, Brazil

Ricardo Elgul Samad
IPEN-CNEN/SP
São Paulo, Brazil

Cláudio Costa Motta
University of São Paulo
São Paulo, Brazil

2025 SBFoton International Optics and Photonics Conference (SBFoton IOPC) | 979-8-3315-9497-8/25/$31.00 ©2025 IEEE | DOI: 10.1109/SBFOTONIOPC66433.2025.11218344

***Abstract*—This work presents a comparative study between single-clad (SCF) and double-clad (DCF) fiber designs, focusing on modal propagation and tolerance to the transverse mode instability (TMI). Analytical solutions for LP_{mn} modes and numerical simulations are used to analyze the transverse intensity distributions and the influence of structural parameters on the TMI onset threshold in high-power fiber lasers. Results show that DCFs exhibit greater tolerance to TMI, attributed to the broader transverse mode distribution in lower-index regions, which enhances optical confinement and thermal dissipation.**

***Index Terms*—Transverse mode instability, LP modes, single-clad fiber, double-clad fiber, high-power fiber lasers**

I. Introduction

Ytterbium-doped optical fibers are widely employed in high-power lasers, however, their performance can be limited by the transverse mode instability (TMI), a thermally induced phenomenon that couples transverse modes and degrades the beam quality [1], [2].

This work investigates the TMI effect in two distinct fiber configurations: a single-clad fiber (SCF), modeled under the weakly guiding approximation (WGA) following the formalism of D. Gloge [3], and a double-clad fiber (DCF), described by the semi-weakly guiding approximation (semi-WGA) as formulated by Tan et al. [4]. The present investigation is restricted to continuous-wave (CW) fiber lasers, although the study of TMI can be extended to pulsed regimes [5].

In the SCF, both the fundamental mode (FM) and higher-order modes (HOMs) remain predominantly confined within the core, enhancing thermal coupling between them. Conversely, in the semi-WGA DCF, the HOMs tend to extend into the inner cladding, reducing modal overlap and potentially mitigating TMI effects. This modal comparison constitutes the main focus of the present study [3], [4].

II. Theoretical Model

In this work, we adopt a cylindrical coordinate system (r, ϕ, z), where r denotes the radial distance from the fiber axis, ϕ is the azimuthal angle, and z corresponds to the longitudinal propagation axis. Fig. 1 schematically illustrates the transverse structures of a SCF and a DCF, characterized by the core radius a, the inner cladding radius b, and the outer cladding radius c. The respective refractive indices are n_1 for the core, n_2 for the inner cladding, and n_3 for the outer cladding, with the relation $n_1 > n_2 > n_3$.

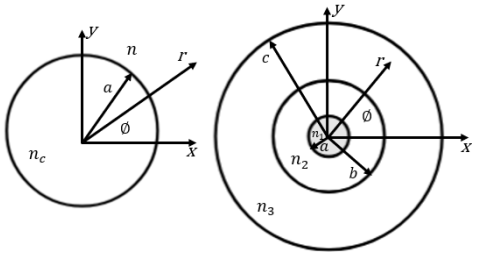

Fig. 1. Schematic cross-sectional view of optical fiber geometries: SCF (left) and DCF (right).

The modal analysis of SCF employs the WGA proposed by Gloge [3], valid for $(n_c - n)/n \ll 1$, where n_c is the core refractive index and n is that of the cladding extending to infinity. In contrast, DCFs require a more precise field modeling and are well described by the semi-WGA approach, as presented by Tan et al. [4], under the condition $n_1 \approx n_2$ and $n_2 > n_3$.

A. Transverse Modal Formulation

SCF (WGA): In Gloge's approximation, the fiber is modeled with two regions: core ($r \leq a$) and cladding ($r > a$). The propagation constant β of any guided mode is confined to the interval $n_c k \geq \beta \geq nk$, where $k = 2\pi/\lambda$ is the vacuum wavenumber and λ is the vacuum wavelength. Under these conditions, the transverse component of the electric field takes the form:

$$E_y(r,\phi) = E_m \begin{cases} [J_m(ur/a)/J_m(u)]\cos(m\phi), & r \leq a \\ [K_m(wr/a)/K_m(w)]\cos(m\phi), & r > a \end{cases} \tag{1}$$

The transverse parameters u and w are related to the propagation constant β by:

$$u = \sqrt{k^2 n_c^2 a^2 - \beta^2 a^2}, \quad w = \sqrt{\beta^2 a^2 - k^2 n^2 a^2}. \tag{2}$$

DCF (semi-WGA): For double-clad fibers, Tan et al. [4] consider three concentric regions. In this case, the propagation constant β is restricted to the interval $n_3 k_0 < \beta < n_2 k_0$. The electromagnetic fields are described by: **for** $0 < r \leq a$**:**

$$E_{y1}(r,\phi) = \frac{A}{J_m(U_1)} J_m\left(U_1 \frac{r}{a}\right)\cos(m\phi), \tag{3}$$

for $a < r \leq b$**:**

$$E_{y2}(r,\phi) = \left[A_{21} J_m\left(U_2 \frac{r}{a}\right) + A_{22} N_m\left(U_2 \frac{r}{a}\right)\right] \cos(m\phi), \tag{4}$$

for $r > b$**:**

$$E_{y3}(r,\phi) = \frac{C}{K_m(W_2)} K_m\left(W_2 \frac{r}{b}\right) \cos(m\phi). \tag{5}$$

The functions J_m, N_m, and K_m represent the Bessel functions of the first kind, second kind (Neumann), and modified Bessel function of the second kind, respectively. The constants A, A_{21}, A_{22}, and C arise from the electromagnetic boundary conditions. The coefficients A_{21} and A_{22} are given by [4]:

$$\begin{aligned} A_{21} &= \frac{A N_m(W_1) - C N_m(U_2)}{J_m(U_2) N_m(W_1) - J_m(W_1) N_m(U_2)}, \\ A_{22} &= \frac{C J_m(U_2) - A J_m(W_1)}{J_m(U_2) N_m(W_1) - J_m(W_1) N_m(U_2)}. \end{aligned} \tag{6}$$

The quantities U_1, U_2, W_1, and W_2 are related through the normalized frequencies [4]:

$$V_1^2 = k_0^2 a^2 (n_1^2 - n_2^2) = U_1^2 - U_2^2, \tag{7}$$

$$V_2^2 = k_0^2 b^2 (n_2^2 - n_3^2) = W_1^2 + W_2^2, \tag{8}$$

where V_1 and V_2 are the normalized frequencies of the core and inner cladding, respectively. These relations highlight the partial penetration of the electromagnetic field into the inner cladding and its attenuation in the outer cladding.

B. Thermal Modal Coupling

Under high-power operation, the stability of the fundamental mode LP_{01} can be compromised by transverse thermal fluctuations that induce coupling to higher-order modes (HOMs), such as LP_{11} and LP_{13}. The total field can be expressed as [6], [7]:

$$E(r,\phi,z,t) = \sum_{m,n} \sqrt{P_{mn}}\, e_{mn}(r,\phi)\, e^{j(\beta_{mn} z - \omega t)}, \tag{9}$$

where P_{mn} is the LP_{mn} mode power and $e_{mn}(r,\phi)$ its normalized transverse profile. Although P_{mn} is z-independent in the field representation, TMI via χ_{mn} couples power between LP_{01} and LP_{mn}, driving their axial evolution. The longitudinal dynamics follow [7]:

$$\frac{dP_{01}(z)}{dz} = \left[- g_{01}\, \Re(\chi_{mn}^*)\, P_{mn}(z) + g_{01} \right] P_{01}(z), \tag{10a}$$

$$\frac{dP_{mn}(z)}{dz} = \left[g_{01}\, \Re(\chi_{mn})\, P_{01}(z) + \gamma_{mn} \right] P_{mn}(z), \tag{10b}$$

where g_{01} is the modal gain of the LP_{01} mode, γ_{mn} is the effective gain of the LP_{mn} mode, and χ_{mn} is the complex thermal coupling coefficient, whose real part determines the effective power transfer between modes.

The power threshold for the onset of TMI can be theoretically estimated as [1]:

$$P_{\mathrm{TMI}}^{\mathrm{thr}} = \frac{\kappa_0 U_\varepsilon^2 (U_\varepsilon^2 - U_s^2)}{4\pi n_{\mathrm{eff}} \left(\frac{dn}{dT}\right) \alpha_s'} \left(\frac{\lambda}{D_0}\right)^2, \tag{11}$$

where $D_0 = 2a$ is the fiber core diameter, κ_0 is the thermal conductivity of silica, U_ε and U_s are the transverse wave numbers of the coupled modes (typically the fundamental mode LP_{01} and a HOM such as LP_{11} or LP_{13}), n_{eff} is the effective refractive index of the fundamental mode, $\mathrm{dn/dT}$ is the thermo-optic coefficient of silica, α_s' represents the effective loss of the fundamental mode, and λ is the operating wavelength.

III. Results and Discussion

The transverse distributions of the LP_{01} and LP_{13} modes in the SCF and DCF are analyzed according to the formalisms of Gloge and Tan [3], [4]. Simulations were implemented in MATLAB (R2016a), adopting typical parameters for high-power lasers: signal wavelength $\lambda_s = 1018\,\mathrm{nm}$, pump wavelength $\lambda_p = 976\,\mathrm{nm}$, ytterbium ion concentration $N_{\mathrm{Yb}} = 6 \times 10^{25}\,\mathrm{m}^{-3}$, and V-number calculated for each fiber type.

TABLE I
Parameters used in the estimation of the TMI threshold

Symbol	SCF	DCF
a (μm)	12.5	12.5
b (μm)	62.5	125
n_1	1.47	1.446612
n_2	1.46	1.445367
n_3	–	1.370214
V-number	12.64	4.43
n_{eff}	1.4697	1.4466
U_{01}	2.23	1.0159
U_{13} (or U_{11})	9.35 (LP13) or 3.08 (LP11)	2.5968
κ_0 (W/mK)	1.38	1.38
dn/dT (K^{-1})	1.2×10^{-5}	1.2×10^{-5}
λ_p (nm)	976	976
λ_s (nm)	1064	1064
N_{Yb} (m^{-3})	6×10^{25}	6×10^{25}
α_s' (m^{-1})	3×10^{-3}	3×10^{-3}
$P_{\mathrm{TMI}}^{\mathrm{thr}}$ (kW)	3.20 (LP11)	2.25 (LP13)

In Tan's model, modal coupling due to TMI does not occur between the LP_{01} and LP_{11} modes because the calculated threshold power $P_{\mathrm{TMI}}^{\mathrm{thr}}$ becomes negative. This results from the U_1 values for the LP_{01} and LP_{11} modes being 1.0159 and 0.7824, respectively, under the fiber dimensional parameters considered. In contrast, Gloge's model predicts initial coupling between the LP_{01} and LP_{11} modes. In this work, however, the coupling between the LP_{01} and LP_{13} modes was adopted for both fiber types. Consequently, in the SCF modeled using Gloge's formalism, the LP_{01} mode couples with nearly all higher-order modes (HOMs) due to TMI, whereas in the DCF, described by Tan's semi-weakly guiding approximation, the coupling is more restricted and does not involve all HOMs.

Figures 2 and 3 show the transverse intensity distribution of the LP_{01} and LP_{13} modes in SCF and DCF. It can be observed that, in the SCF, both the fundamental mode (FM) and higher-order modes (HOMs) remain strongly confined to the core. In contrast, in the DCF, the HOMs exhibit greater radial extension, with significant penetration into the inner cladding. This spreading reduces the spatial overlap with the FM, which may mitigate modal coupling induced by TMI.

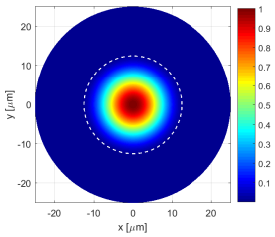

(a) LP_{01} – SCF

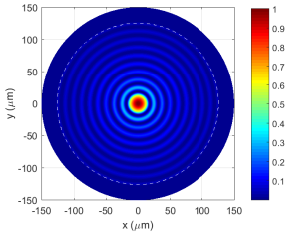

(b) LP_{01} – DCF

Fig. 2. Transverse intensity distribution of the LP_{01} mode in the SCF (a) and DCF (b).

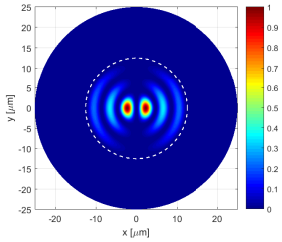

(a) LP_{13} – SCF

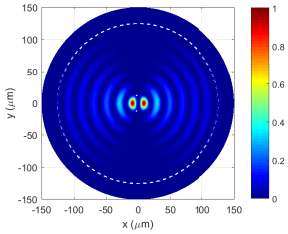

(b) LP_{13} – DCF

Fig. 3. Transverse intensity distribution of the LP_{01} mode in the SCF (a) and DCF (b).

The evolution of the modal superposition induced by TMI was simulated for the LP_{01}–LP_{13} pair in SCF and DCF. The coupling between the modes is modeled by a nonlinear coefficient χ_{mn} [7], which represents the thermal coupling responsible for the energy transfer from the FM to the HOMs. Figs. 4 and 5 show the transverse mode distributions under the influence of TMI. In both cases, it is observed that the LP_{01} mode transfers approximately 30% of its power to the LP_{13} mode along the propagation, evidencing significant thermal coupling between the modes.

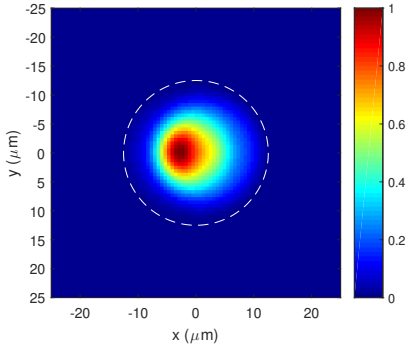

Fig. 4. Evolution of modal power between the LP_{01} and LP_{13} modes in an SCF, due to thermal coupling induced by the TMI effect.

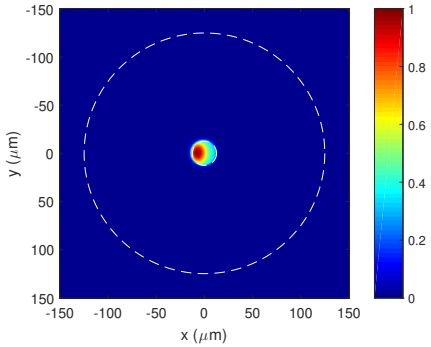

Fig. 5. Evolution of modal power between the LP_{01} and LP_{13} modes in a DCF, due to thermal coupling induced by the TMI effect.

In the SCF, the modal coupling induced by TMI occurs predominantly in the core, where the FM and HOMs remain strongly confined (Fig. 4). In contrast, in the DCF, the instability manifests near the core–inner cladding interface, as some HOMs penetrate the inner cladding (Figs. 2–3(b)). This characteristic favors the propagation of HOMs outside the core, resulting in a more dispersed transverse TMI pattern (Fig. 5).

Conclusion

The SCF, modeled by Gloge's formalism based on the WGA, exhibits strong confinement of both the FM and HOMs within the fiber core region, which promotes thermal coupling between these modes and increases its susceptibility to TMI. In contrast, the DCF, described by the semi-WGA approach according to Tan, has HOMs that penetrate more into the inner cladding, reducing the efficiency of modal coupling. However, this formulation may overestimate the reduction of thermal modal coupling, leading to a theoretically lower TMI threshold. The modeling highlighted the importance of the modal profile in mitigating TMI and suggests future inclusion of longitudinal temperature variations to improve the description of modal dynamics and instability threshold.

References

[1] M. N. Zervas, "Transverse mode instability analysis in fiber amplifiers," in *Fiber Lasers XIV: Technology and Systems*, vol. 10083. SPIE, 2017, pp. 115–123.

[2] E. S. Cardoso, R. E. Samad, and C. C. Motta, "Refractive index change analysis in a high-power Yb-doped double-clad fiber laser," in *2021 SBFoton International Optics and Photonics Conference (SBFoton IOPC)*. IEEE, 2021, pp. 1–4.

[3] D. Gloge, "Weakly guiding fibers," *Applied optics*, vol. 10, no. 10, pp. 2252–2258, 1971.

[4] X. Tan, X. Liu, W. Zhao, C. Li, Y. Wang, and J. Li, "Modal characteristics analysis of a doubly clad optical fiber with semi-weakly guiding approximation," *Optics Communications*, vol. 294, pp. 148–155, 2013.

[5] K.-H. Lee *et al.*, "Transverse mode instability induced by stimulated brillouin scattering in a pulsed single-frequency large-core fiber amplifier," *Applied Optics*, 2015.

[6] D. Gloge, "Optical power flow in multimode fibers," *Bell System Technical Journal*, vol. 51, no. 8, pp. 1767–1783, 1972.

[7] L. Dong, "Stimulated thermal rayleigh scattering in optical fibers," *Optics Express*, vol. 21, no. 3, pp. 2642–2656, 2013.